Chemical Engineering Journal 148 (2009) 506–516

Contents lists available at ScienceDirect

Chemical Engineering Journal

journal homepage: www.elsevier.com/locate/cej

Multifluid Eulerian modelling of a silicon Fluidized Bed Chemical Vapor Deposition process: Analysis of various kinetic models

N. Reuge*, L. Cadoret, B. Caussat*

Laboratoire de Génie Chimique, UMR CNRS 5503, ENSIACET/INPT, 5 rue Paulin Talabot, BP 1301, 31106 Toulouse Cedex 1, France

ARTICLE INFO

Article history:
Received 24 July 2008
Received in revised form 11 December 2008
Accepted 11 December 2008

Keywords:
Fluidized bed
CVD
CFD
Kinetics
Silicon
Silane

ABSTRACT

Using the multifluid Eulerian code MFIX, the silicon Fluidized Bed Chemical Vapor Deposition process from silane (SiH_4) has been modelled under transient conditions. In order to constitute an experimental database, a preliminary experimental study has been performed using a bed of Geldart's group B particles.

After a detailed analysis and comparison of the kinetic models available in the literature, four of them have been implemented in the MFIX code and two hydrodynamic models have been tested. 3-D simulations have shown that a strong interaction exists between the bed hydrodynamics, heat and reactive mass transfers and that Si deposition from silane mainly occurs in the dense zones of the bed whereas the unsaturated species silylene (SiH_2) forms in bubbles and slugs and leads to Si deposition mainly at their periphery; its contribution to deposition can be locally as high as that of SiH_4. The average contribution of SiH_2 to deposition increases with the inlet concentration of silane and can reach 30%. The kinetic models derived from the law of Furusawa et al. and from the data compiled by Buss et al. and the hydrodynamic model based on the true granular energy equation and the Princeton solid phase stress model have revealed to be the most appropriate ones for the conditions tested.

1. Introduction

Over the past years, the solar photovoltaic industry has experienced a strong expansion due to the inexhaustible and clean characteristics of solar energy [1]. This development explains the significant increase in the demand for solar grade (SG) silicon since polycrystalline silicon based solar cells are the predominant solar cell technology [2].

The Fluidized Bed Chemical Vapor Deposition (FBCVD) process using silane (SiH_4) as silicon CVD precursor represents one of the most interesting technologies to produce SG silicon [3]. The main principle of the process is to grow small seed powders into larger product-size particles via silicon deposition from silane on the grains.

A major challenge is to control the particle growth process in order to keep a steady-state average particle size [3]. The understanding of the chemical and physical phenomena involved during silicon deposition is of main importance. Moreover, one of the most important obstacles for the widespread application of this technology is the expensive and time-consuming scale-up of the reactor [1]. In this framework, the development of an accurate model accounting for the hydrodynamics, heat and reactive mass transfers existing inside the FB appears as an efficient way of progress.

Silane is the CVD precursor for which the chemical reaction pathways and associated kinetics have been the most deeply studied. Lai et al. [4] were the first ones to develop a FBCVD model for silicon deposition. They employed a modified version of the bubbling bed model of Kato and Wen [5] and the kinetic laws of Hogness et al. [6] and of Iya et al. [7]. By simulating the experimental results of Hsu et al. [8], they could not explain the influences of operating conditions on the process behaviour. Furusawa et al. [9] established specific kinetic laws for silicon FBCVD from silane, quantifying on one hand silane heterogeneous decomposition and on another hand homogeneous phenomena supposed to lead to silicon nuclei (fines) formation. They combined these laws with a modified version of the Kunii and Levenspiel model [10] in order to determine the regions of fines formation into the bed and to explain the effect of the inlet silane concentration on fines production. They compared their results with the experimental data of Hsu et al. [8], and they obtained reasonable agreement for inlet concentration above 20 vol.%; below, their calculations over-evaluated fines formation. They explained this discrepancy by the fact that at low silane concentration, the rate of fines formation is small and then their catching by the bed particles is easy. Caussat et al. [11] modified four bubbling bed models to account for the increase in moles number due to chemical reactions and then in gas flow velocity occurring during silane pyrolysis. By using the law of Furusawa et al. [9] to represent the heterogeneous decomposition of silane,

* Corresponding authors. Tel.: +33 5 34615252; fax: +33 5 34615253.
E-mail addresses: reuge@free.fr (N. Reuge), brigitte.caussat@ensiacet.fr (B. Caussat).

1385-8947/$ – see front matter.
doi:10.1016/j.cej.2008.12.017

Nomenclature

D	column diameter (m)
D_i	diffusion coefficient of the species i in the carrier gas ($m^2\ s^{-1}$)
F_i	molecular incident flux of the species i (molecules $m^{-2}\ s^{-1}$)
H	expanded bed height (m)
H_0	bed height at packing (m)
k_f	kinetic constant of fines formation ($m\ s^{-1}$)
k^{het}	kinetic constant of an heterogeneous chemical reaction ($m\ s^{-1}$)
k^{hom}	kinetic constant of an homogeneous chemical reaction (s^{-1})
M_i	molar mass of the species i ($kg\ mol^{-1}$)
P_i	partial pressure of the species i (Pa)
R	perfect gas constant ($J\ mol^{-1}\ K^{-1}$)
T	gas temperature (K)
T_{bed}	bed temperature defined by (15) (K)
T_s	temperature of the solid phase (K)
U_g	superficial gas velocity ($m\ s^{-1}$)
U_{mf}	superficial gas velocity at minimum fluidization ($m\ s^{-1}$)
V_s	total volume of the solid phase (m^3)
$X^0_{SiH_4}$	inlet mass fraction of silane

Greek letters

ε_s	solid fraction
γ_i	sticking coefficient of the species i
σ_{vp}	internal surface area of the bed (m^{-1})
τ_1, τ_2, τ_3	dimensionless numbers defined by relations ((12)–(14))

they obtained a reasonable agreement with their experimental data especially for the Kato and Wen model. In a second step, they added the kinetic laws of Fayolle [12] to this model in order to partially represent homogeneous mechanisms of silane pyrolysis accounting for the appearance of silylene (SiH_2), and polysilanes in the gas phase. New insights in the chemical mechanisms of silicon deposition have thus been obtained.

It is worth noting that the bubbling bed models present strong limitations to accurately represent FBCVD processes. For instance, they consider the FB as composed of two or three phases either perfectly mixed or in plug flow, which is not very realistic. Their interphase mass transfer coefficients have been empirically determined in the seventies, most often in absence of chemical reaction. These coefficients are then of low precision when high concentration gradients exist: we will see that this is the case in the silicon FBCVD process from silane.

More recently, White et al. [3] established a model of size distribution for SG silicon deposition from silane in FB with an approach derived from the classical population balance. They used the kinetics of Iya et al. [7] for the heterogeneous decomposition of silane and that of Hogness et al. [6] for its homogeneous pyrolysis. By comparison with experimental data, they fixed appropriate values of adjustable parameters to accurately predict fines scavenging and particle aggregation. Pina et al. [13] simultaneously solved the fundamental balance equations in a spouted bed and a population balance equation to describe SG silicon particles production from silane by CVD in a spouted bed. They considered in their model possible agglomeration, seeds inflows and/or particles outflows. They obtained reasonable predictions of experimental data, in particular silane conversion, particle growth rate and size distribution, after adjustment of a sole parameter (an agglomeration efficiency).

Due to the rapid advances in multiphase flow mechanics and in computational capabilities, these global models (i.e. those of Kato and Wen or Kunii and Levenspiel) can today be replaced by more accurate approaches using computational fluid dynamics (CFD). However, the development of such multiphase flow simulation codes is still a topic of current research due to the complexity of fluidized gas–solid systems. For example, there is still no general agreement on the appropriate closure models [14], and terms such as the solid phase stresses or the interphase momentum transfer.

At the present time, only Guenther et al. [15] modelled by CFD silicon FBCVD from silane. They implemented into the MFIX code [16] the heterogeneous and homogeneous kinetic laws used by Caussat et al. [11] in order to simulate the experimental data of these authors. Their calculations allowed to predict local mass fractions of the various species involved and their calculated silane conversions were quite close to the experimental data.

In the present work, the CFD code MFIX has been used to simulate in transient conditions a lab-scale silicon FBCVD process from silane. First, experiments of silicon FBCVD have been performed on Geldart's group B particles to constitute an experimental database for the model validation. The setup, operating conditions and results obtained will be briefly described. Then, a detailed analysis and comparison of the homogeneous and heterogeneous kinetic models available in the literature will be presented to select the most appropriate ones for our conditions. Results of the MFIX simulations will be analysed and compared with experiments for four different kinetic models and two hydrodynamic models.

2. Experimental

The experimental setup has been presented in details elsewhere [17]. Silane, diluted in nitrogen (N_2), was used as precursor leading to Si deposition. Powders were Geldart's group B alumina particles (Al_2O_3) with a mean Sauter diameter of 329 μm, as measured by laser granulometry (MasterSizer2000). The standard deviation of their volume size distribution was of 77 μm. The alumina particles revealed to be non-porous, therefore their bulk density was equal to the density of alumina (i.e. 3900 kg/m^3). Since the specific surface area of the powders is an important parameter for the deposition, we cautiously investigated it. From shape factor measurements by laser granulometry, we could estimate a value of about 0.55 for the sphericity of the particles and a surface area of about 33,160 m^2/m^3 of full material (or 8.5×10^{-3} m^2/g). The minimum fluidization velocity of these powders U_{mf} was found equal to 12.5 cm/s at 20 °C and to 8 cm/s at 600 °C.

The operating conditions tested and the experimental results are given in Table 1. The operating parameters were chosen so that the silane conversions were lower than 100% in order to obtain an experimental database really discriminating for the model. Theoretical thicknesses and conversions of silane were deduced from the deposited weights. Elutriation was negligible. Uncertainties of ±10% could affect the conversions measured.

When using 800 g of powders (for all runs except run A12), and a gas velocity around 30 cm/s, the mean bed height has been roughly estimated as equal to 30 cm (from measurements performed in a glass column at ambient temperature, see [18]). The cooling of the region below the distributor was responsible for significant thermal gradients all along the bed height during silicon deposition [17]. As temperature is a key parameter for CVD, and in order to reach a maximal precision in the simulations, thermal profiles along the column axis have been measured by translating a thermocouple in a gorge worked inside the column walls and in an inner tube placed in central position along the reactor. Thermal profiles obtained for each

Table 1
Processing parameters for Si deposition on alumina particles and experimental results.

Run	Mean temperature in the axial tube [0–40 cm] (°C)	U_g/U_{mf}	Initial weight of powders (g)	Inlet mass fraction of silane	Run duration (min)	Weight of injected Si (g)	Weight of deposited Si (g)	Silane conversion (%)	Calculated thickness of deposited Si (μm)	Calculated Si deposition rate (nm/min)
A5	615	4.2	800	0.0615	25	20.3	16.4	80.8	1.0	42
A7	605	4.5	800	0.1185	20	36.8	24.2	65.7	1.5	77
A11	585	4.1	800	0.077	40	41	24.4	59.5	1.5	38
A12	572	4.1	1300	0.078	40	41.4	36.3	87.7	1.4	36
A13	610	4.1	800	0.0275	60	21.9	21.2	96.8	1.4	23

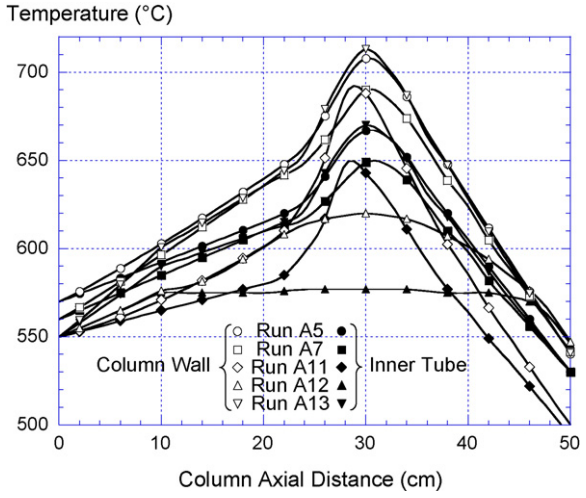

Fig. 1. Thermal profiles measured at the column walls and in the inner tube.

run are reported in Fig. 1. It appears that the temperature increases from the distributor to a height of 30 cm and then sharply decreases. Logically, the column walls are always hotter (several tens of °C) than the inner tube. For all runs except run A12, the mean temperature gradient for heights between 0 and 30 cm is around +5 °C/cm at the column walls whereas it is lower, i.e. +3 °C/cm, in the inner tube. It decreases to only +2.3 °C/cm at the column walls and +0.8 °C/cm in the inner tube by increasing the initial bed weight by a factor 1.6 (run A12). Indeed, the total surface of contact between the walls and the powders increases with the FB weight (and height) and therefore the heat transfer is enhanced.

Table 1 shows that the deposition rate varies between 23 and 77 nm/min, increasing with temperature (runs A11 and A5) and with inlet mass fraction of silane (runs A13, A5 and A7). The silane conversion logically increases with temperature (runs A11 and A5) and with the initial FB weight (runs A11 and A12) but decreases with the inlet mass fraction of silane (runs A13, A5 and A7).

For the conditions tested, the size distribution of powders has not been modified by the deposition indicating that no agglomeration of particles occurred. SEM analyses revealed that deposition was uniform on powders. These are now well-established results for silicon FBCVD from silane on Geldart's group B particles.

3. Multifluid Eulerian modelling of the process

3.1. General model features

The CFD open-source code MFIX [16], a benchmark tool for the simulation of gas–solid systems, was used for this study. Calculations were performed using the continuum model, the drag law of Syamlal–O'Brien [19,20], the kinetic theory of granular materials with an algebraic or differential form for the granular temperature equation for the solid phase stress tensor in the viscous regime. To calculate the solid phase stress tensor in the plastic regime, both Schaeffer [21,22] and Princeton [23] models were tested. The summary of the governing equations is given in [17], the expressions of the granular stress models employed are given in [18] and the details can be obtained from MFIX documentation [19,21].

The numerical method employed for time discretization is the implicit backward Euler method; for spatial discretization the Superbee method (second order) was chosen here (see [18,24–26] for further precisions).

As shown in [15,17,18,27], performing 3-D calculations is necessary to reasonably predict the hydrodynamics of FB. Compared

with simulations reported in our previous studies [17,27], based on the same experimental database, the present work presents several significant improvements as follows:

- the description of heat transfer in the bed has been improved by solving the energy equations (given in [21]) for the two phases and by implementing a model of Rosseland [28] to describe the radiation of heat between bed particles that form an optically thick medium;
- an improved hydrodynamic description has been tested using the Princeton model [23] instead of the Schaeffer one [21,22] for solid phase stresses calculations. The Princeton model requires the use of the true granular energy equation (partial differential equation) whereas its algebraic approximated form [19,21] can be used with the Schaeffer model (as done by default in MFIX); both approaches have been used and compared in this study;
- the sphericity of particles has been considered in order to better estimate the specific surface of powders available for deposition;
- the gaseous species transport has been better described by implementing an improved model of species diffusion: the Wilke approximation [29,30] of multicomponent diffusion was used instead of the constant dilute approximation.

Finally, we have studied various detailed kinetic models of silane chemistry, as presented in Section 4.

3.2. Powder parameters

For the simulation, a monodisperse powder of diameter 329 μm (i.e. the measured Sauter diameter) was considered, with a volume surface area of 33,160 m^2/m^3 (see Section 2). The internal angle of friction was fixed to 40°, which is the experimentally determined angle of repose of the powder. Indeed, for non-cohesive powders, these two parameters are identical [31]. Since we did not find any data in the literature for the restitution coefficient for the collisions of alumina particles, the default value of 0.8 was used and we showed in [18] that the bed hydrodynamics was correctly reproduced with such a value for this powder. The measured minimum fluidization velocity U_{mf} at 600 °C, i.e. 8 cm/s, was used to adjust the coefficients of the Syamlal–O'Brien drag correlation [20] (which is at the limit of its range of validity for these conditions); so the model agrees with experiment at minimum fluidization.

3.3. Processing parameters and boundary conditions

The operating conditions simulated are those of Table 1. Experimental thermal profiles (see Section 2 and Fig. 1) were included as boundary conditions (BCs) at the column walls and at the inner tube walls in the simulations. Gas and solid temperatures at the column entrance were adjusted to correspond to the thermal profiles. As walls BCs, no slip for gas was applied; when the true granular energy equation was used (i.e. with the Princeton model), Johnson & Jackson partial slip for solids was applied [32] whereas when the algebraic equation of granular energy equation was used (i.e. with the Schaeffer model), free slip was applied (Johnson & Jackson partial slip cannot be applied with the algebraic equation of granular energy).

Some preliminary 3-D calculations showed that grid independent results were achieved in terms of bed expansion, height of fluctuation of the bed surface, frequency of fluctuation and silane conversion by using 250 cells along the axial direction for a height of 0.6 m, 15 cells along the radial direction for the half diameter, and 6 angular cells.

4. Models of silane chemistry

Silane pyrolysis occurs from a temperature of about 350 °C [6]. In an inert carrier gas, silane and the gaseous species produced by its pyrolysis can react on hot temperature surfaces to form silicon deposits. Two modelling approaches can be envisaged:

- The first one consists in modelling all the decomposition/pyrolysis homogeneous chemical reactions to know the composition of the gaseous phase near the deposition areas, then in identifying the species that actually lead to deposition and finally in modelling these chemical heterogeneous reactions.
- The second one consists in using a global model that directly predicts the silicon deposition rate as a function of the silane concentration. The homogeneous chemistry is ignored and the unique heterogeneous reaction considered is:

$$SiH_4 \xrightarrow{k^{het}} Si_{(s)} + 2H_2 \qquad (R_{het})$$

Global models are easier to use but their level of accuracy is lower.

Another phenomenon that can be important to consider is the formation of fine particles in the gas due to homogeneous nucleation. These nucleated particles can encounter the deposition surfaces and eventually incorporate into the deposits. In FBs, fines can form essentially in bubbles where the homogeneous chemistry is not inhibited by the heterogeneous one [33] and their amount increases as a function of U_g/U_{mf}, i.e. with the bubble size [34].

4.1. Global models

From experiments of Si deposition performed at atmospheric pressure in fluidized or fixed beds, Rohatgi et al. [34] and then Iya et al. [7] seem to have been the first authors to propose global kinetics of Si deposition from silane on powders. But their processing parameters (hydrogen as carrier gas, high inlet mass fractions of silane) are very far from the ones used for our experiments (see Section 2). So we did not use their kinetics.

Note that in their modelling study of FBCVD, Lai et al. [4] claim to use the kinetics given by Iya et al., but it seems that Lai et al. mistook by using a pre-exponential factor two times higher. Pina et al. and White et al. [1,3] used the erroneous kinetics written in the paper of Lai et al. for their global modelling study of FBCVD.

For silane diluted in argon, with inlet mass fractions of SiH_4 between 0.5% and 10% (or SiH_4 partial pressures between 500 and 10^4 Pa), for temperatures between 575 and 675 °C, Furusawa et al. [9] performed experiments of Si deposition in a fixed bed at atmospheric pressure and deduced the following kinetic expression:

$$k^{het} = \frac{2.15 \times 10^8 \exp(-19,1500/RT)}{1 + 3.4 \times 10^{-5} P_{H_2} + 7.6 \times 10^{-6} \exp(32,900/RT) P_{SiH_4}} \ (m\,s^{-1}) \qquad (1)$$

where P_{H_2} and P_{SiH_4} are the partial pressures of hydrogen and silane. Note that all the activation energies given in this paper are expressed in J mol^{-1}.

The three global kinetic laws cited here provide quite different activation energies and apparent reaction orders of silane. And even in their common range of validity, they lead to significantly different values of silicon deposition rate (of a factor from 2 to 4). This can be explained by the fact that they were determined neither from the same specific surface areas of powders nor from the same processes (fixed or fluidized bed). Indeed, on one hand, the fact that Rohatgi et al. worked with a vigorously bubbling fluidized bed and that Iya et al. with a fixed bed formed of a powder of low specific surface area (particles diameter equal to 1595 μm) are factors that can more or less increase the influence of the homogeneous chemistry and

hence have an effect on the global deposition rates. On the other hand, Furusawa et al. worked with a high specific surface area fixed bed (particles diameter equal to 385 μm), that tends to promote the heterogeneous chemistry.

Furusawa et al. have also estimated the formation rate of fines by working in the same operating conditions but with an empty reactor. They propose the following global homogeneous kinetics [9]:

$$k_f = 2.14 \times 10^{13} \exp\left(-\frac{221,300}{RT}\right) \ (\mathrm{s}^{-1}) \quad (2)$$

In their modelling study of FBCVD, Lai et al. [4] estimated the formation of fines using the kinetics proposed by Hogness et al. [6] for silane homogeneous decomposition at temperatures between 380 and 490 °C. At typical FB temperatures (around 600 °C), this kinetics is higher than the kinetics (2) by a factor of about 2, so one can think it would tend to overestimate much the formation rate of fines. However, the kinetics of Hogness has been used again in some recent modelling studies [1,3] to estimate the formation rates of fines.

Estimating the formation rate of fines is not sufficient, one must be able to predict the proportion of them that are incorporated into the deposit, which is rather difficult. Hsu et al. [35] and Lai et al. [4] attempted to do it. Pina et al. [1] adjusted their calculations on experiments by adjusting the scavenging of fines. Overall, the scavenging of fines by particles in dense FBs seems to be important [1,35], varying between 50% and 66% in the study of Hsu et al. [35].

4.2. Detailed models

4.2.1. Homogeneous kinetics

The first homogeneous chemical reactions occurring during silane pyrolysis are the following [36]:

$$SiH_4 \underset{k_{-1}^{hom}}{\overset{k_1^{hom}}{\rightleftarrows}} SiH_2 + H_2 \quad (R_1, R_{-1})$$

$$SiH_4 + SiH_2 \underset{k_2^{hom}}{\overset{k_{-2}^{hom}}{\rightleftarrows}} Si_2H_6 \quad (R_{-2}, R_2)$$

$$Si_{n-1}H_{2n} + SiH_2 \underset{k_n^{hom}}{\overset{k_{-n}^{hom}}{\rightleftarrows}} Si_nH_{2n+2} \quad (R_{-n}, R_n)$$

Silane first decomposes to give the highly reactive chemical species silylene (SiH_2). Simultaneously, silane decomposition can lead to another radical species, SiH_3, but in insignificant amount, even at very high temperature [37]. The higher the temperature and the longer the residence time of the gas phase in hot zones, the more advanced the silane pyrolysis and the more numerous are the reactions (R_{-n}, R_n) to be considered: the model of Coltrin et al. counts 27 reactions [36].

At atmospheric pressure, the first reaction (R_1) is in its fall-off zone and its kinetics difficult to determine with accuracy. The most recent kinetics proposed for (R_1) are those of Ho et al. [38] and Dollet et al. [37]. They were theoretically determined for a wide range of temperatures and have been relatively successfully compared with experiments around 600–650 °C. However, the authors used different methods (RRKM and QRRK models) to determine them and they obtain significantly different results: at 600 °C, these kinetics differ by a factor of 1.6. Since no method is a priori better than the other, we chose to use the kinetics of Coltrin et al. [36] which leads to intermediate results in the range of temperatures studied. It is given by:

$$k_1^{hom} = 1.09 \times 10^{25} T^{-3.37} \exp\left(-\frac{256,232}{RT}\right) \quad (3)$$

Note that the kinetics of fines formation k_f given by Furusawa et al. [9] is higher than k_1 (by a factor two at 600 °C). This is not contradictory a priori if we consider that silane molecules can directly condense in the gaseous phase to form clusters, but this is not an assumption retained in the most recent models about fines formation [39–41].

For (R_2), Coltrin et al. [36] give the following kinetics:

$$k_2^{hom} = 3.24 \times 10^{29} T^{-4.24} \exp\left(-\frac{242,834}{RT}\right) \quad (4)$$

Backward reaction rates are easily determined from forward reaction rates and thermochemical properties of the species involved [42]. We will show in Section 4.3 that it is useless to consider the subsequent species and homogeneous reactions involved in silane pyrolysis for the calculations.

4.2.2. Heterogeneous kinetics

To determine the heterogeneous kinetics of the reactions leading to Si deposition is difficult because it is not experimentally simple to isolate one specific species in order to measure its deposition rate. On the basis of experiments performed by [43] and [44], Coltrin et al. [45] seem to be the first one to propose a sticking coefficient for Si deposition from silane at atmospheric pressure between 550 and 750 °C. From their work and from the relation given by [42,46], the following kinetics can be deduced:

$$k_{SiH_4}^{het} = 0.35\sqrt{T} \exp\left(\frac{-78,152}{RT}\right) \quad (5)$$

with a reaction order of 1. However, from the studies of Buss et al. [47] and Wang et al. [48], the sticking coefficient γ_{SiH_4} of silane depends on its incident flux F_{SiH_4}, which is not compliant with a reaction order of 1.

From numerous experimental studies of low pressure CVD (LPCVD) of Si from silane performed at a deposition temperature of 625 °C, Buss et al. [47] calculated the sticking coefficient of silane as a function of its incident flux (see Fig. 9 of [47]).

We have reproduced the results of Buss et al. in Fig. 2, where the sticking coefficient is presented as a function of the silane partial pressure. The data compiled by Buss et al. concern silane partial pressures between 0.1 and 100 Pa. Linearly fitting these log-log data for pressures higher than 1 Pa, we obtained the following expression for the sticking coefficient:

$$\gamma_{SiH_4}(625\,^\circ\mathrm{C}) = 3.718 \times 10^{-4} P_{SiH_4}^{-0.7325} \quad (6)$$

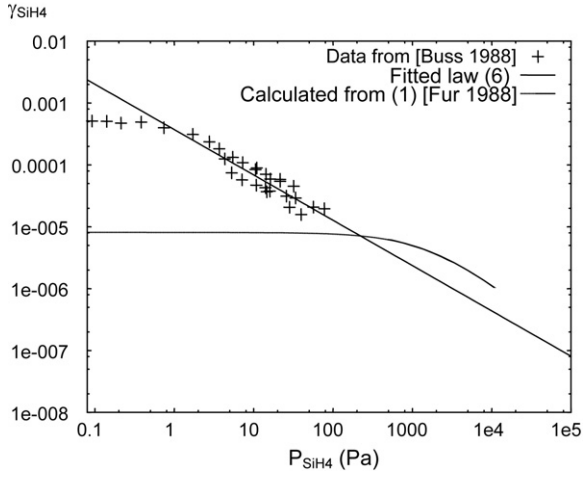

Fig. 2. Silane sticking coefficient *vs.* silane partial pressure at 625 °C.

It leads to the following kinetics:

$$k^{het}_{SiH_4}(625\,^\circ C) = 7.165 \times 10^{-2} P^{-0.7325}_{SiH_4} \quad (7)$$

Then, as explained by Breiland and Coltrin [49], several experimental studies of LPCVD performed around 600 °C [50–52] have shown that the activation energy of the Si deposition from pure silane would be of about 40 kcal/mol (i.e. 167 kJ/mol). Therefore, we can deduce the following kinetic law:

$$k^{het}_{SiH_4} = 3.9 \times 10^8 \exp\left(-\frac{-167,370}{RT}\right) P^{-0.7325}_{SiH_4} \quad (8)$$

and then the reaction order is of 0.27.

Breiland and Coltrin [49] applied the same reasoning from the data of Buss et al. but considered a constant silane partial pressure (i.e. 17.3 Pa, corresponding to the inlet value of their experiments performed in helium as carrier gas and at atmospheric pressure). They implemented the obtained kinetics and the other reactions of silane pyrolysis in their simulation and found a good agreement with experiments whereas it was not the case using the kinetics (5). The kinetic law (5) was therefore invalidated. So, for our processing conditions, it has been assumed that the kinetics (8) is valid to a maximum silane partial pressure of 10^4 Pa.

Another possibility is to use the global kinetics (1) as the kinetics for Si deposition from silane $k^{het}_{SiH_4}$, as done by [11]. Since Furusawa et al. worked in a fixed bed (i.e. with no large gaseous space between particles) and with a relatively high specific surface area, we can assume that the homogeneous chemistry was completely inhibited and the contribution to deposition of other species negligible. However, reporting the kinetics (1) in Fig. 2, significant differences appear with the kinetics (8). On one hand, for P_{SiH_4} higher than 300 Pa, the kinetics (1) becomes higher than the kinetics (8) by a factor two in its range of validity (i.e. for P_{SiH_4} lower than 10^4 Pa): this could be due to a contribution to deposition of homogeneously born species during experiments of Furusawa et al. or to the uncertainty of law (8) between 100 and 10^4 Pa. On the other hand, for P_{SiH_4} lower than 300 Pa, the kinetics (1) becomes lower and lower than the kinetics (8). The invalidity of the kinetics (1) at very low pressures has not a radical influence on a global point of view as long as it is used with a minimum inlet P_{SiH_4} of 500 Pa.

Then, from Coltrin et al. [45] and for most of the authors, all radical species coming from silane pyrolysis have a sticking coefficient of 1. Therefore, the kinetics of silylene deposition is given by:

$$k^{het}_{SiH_2} = 13.28\sqrt{T} \quad (9)$$

At last, from several studies [36,38,47], the sticking coefficient of disilane would be 10 times higher than the silane one. Therefore, we could use the following kinetics:

$$k^{het}_{Si_2H_6} = 3.9 \times 10^9 \exp\left(-\frac{167,370}{RT}\right) P^{-0.7325}_{Si_2H_6} \quad (10)$$

But for Moffat and Jensen [53] and Gates et al. [54], it would be of 1. This corresponds to:

$$k^{het}_{Si_2H_6} = 9.2\sqrt{T} \quad (11)$$

Detailed models considering several elementary steps exist in the literature to describe the deposition mechanisms of silane and disilane [38,47,55], but implementing these steps in a multifluid Eulerian model such as MFIX would be difficult. This is also the case for the detailed models describing the formation of fine particles by nucleation [39–41].

4.3. Assumptions and limitations of the Eulerian approach

Using these detailed chemistry models, preliminary calculations with MFIX showed that, independently of the conditions in our whole operating range and of the heterogeneous kinetics used for disilane, i.e. (10) or (11), the amount of disilane produced was negligible and the contribution to the deposition completely insignificant. The simulations presented in the next section do not take into account the subsequent species and homogeneous reactions involved after (R_1) and the reverse (R_{-1}). The amount of silylene is significant in our processing conditions and calculations will show its contribution to deposition.

Although the CFD 3-D modelling represents a considerable improvement compared to the global models used earlier (see introduction [5,10]), the Eulerian approach still possesses some strong limitations and assumptions. Let us consider for the species i the characteristic times of diffusion τ_1, of convection τ_2, and of heterogeneous reaction τ_3 given by:

$$\begin{cases} \tau_1 = \left(l_p/2\right)^2 D_i^{-1} & (12) \\ \tau_2 = l_p\left(u_g - u_p\right)^{-1} & (13) \\ \tau_3 = \left(k_i^{het}\sigma_{V_p}\right)^{-1} & (14) \end{cases}$$

where l_p is the distance between two particles (which is equal to about the particle diameter d_p if the void fraction is of 0.5), D_i the diffusion coefficient of the species i in the carrier gas, u_g the gas velocity, u_p the particles velocity, k_i^{het} the heterogeneous kinetic constant of the species i and σ_{V_p} the internal surface area of the bed. Since the Eulerian approach considers uniform species concentration at the particles scale and then ignores local transport by diffusion and convection at this scale, it implicitly assumes that either τ_1 or τ_2 is much lower than τ_3. For our processing conditions, we find characteristic times τ_1 and τ_2 of about 10^{-4} s. τ_3 is about 1 s for silane and 10^{-7} s for silylene. Consequently, the Eulerian approach is convenient with the silane kinetics but no longer with the silylene one. A strictly rigourous modelling of this FBCVD process would require to consider the transport phenomena at the particle scale and this could significantly modify the results. To our knowledge, a Lagrangian modelling of such phenomena for a full fluidized bed is not presently feasible due to computational limitations.

If the transport phenomena at the particle scale were taken into account, the deposition rate of silylene would appear to be locally limited by diffusion. Thus, unlike the preliminary calculations aforementioned, a significant part of silylene would react with silane to form disilane, trisilane, etc..., and fines. Because of the limitations of the Eulerian approach and since the species resulting from the homogeneous chemistry are much more reactive than silane, we will assume that all of them are present in the gas phase in the form of silylene as implicitly supposed initially. This is a strong but unavoidable assumption.

5. Results

To simulate the five runs detailed in Table 1, calculating 15 s of process time was necessary to reach a temporally averaged pseudo thermal equilibrium over the bed. However, gas and solid temperatures continued to fluctuate due to the intrinsic transient nature of the process (see next section). To account for this, the runs were simulated for additional 8 s with the energy equation still activated. When just changing of chemistry model from one case to another, we verified that it was not necessary to redo the first calculation stage of 15 s. In average, computing 8 s of process time took a total computation time of 1300 CPU hrs, i.e. 2 weeks using 4 CPU's. This

could be reduced to about 1000 CPU hrs using the algebraic form of the granular temperature equation (instead of its differential form) with the Schaeffer model.

We will use the following notations to identify the chemistry models tested in the simulations:

- GC: global chemistry, kinetics (1),
- COL: detailed chemistry, homogeneous kinetics (3), heterogeneous kinetics (5) and (9),
- BUS: detailed chemistry, homogeneous kinetics (3), heterogeneous kinetics (8) and (9),
- FUR: detailed chemistry, homogeneous kinetics (3), heterogeneous kinetics (1) and (9).

and the following notations to identify the hydrodynamic model used:

- HM1: Schaeffer model, algebraic expression of the granular energy equation,
- HM2: Princeton model, true expression of the granular energy equation.

5.1. Local results

Instantaneous fields of void fraction and solid phase temperature calculated after 5 s of deposition for run A5 with the model BUS/HM2 are presented in Fig. 3(a and b) respectively. Fig. 3(a) shows that a slug of gas occupies the upper part of the bed (which is at its maximum expansion) whereas bubbles are coalescing above the distributor to form another slug. The bed is clearly in the slugging regime for such high gas velocity (about 30 cm/s) and H_0/D ratio, as observed experimentally at ambient temperature in a glass column [18]. In Fig. 3(b), it can be observed that the solid phase temperature increases axially from about 600 to 610 °C at this run time. When the bed is at its minimum expansion, the column walls may radiate on the inner tube above the bed, and this is why the tube is very hot in its upper part and heats easily the few particles present at the center of the slug on (Fig. 3b). The corresponding fields of silane and silylene mass fractions are presented in Fig. 4(a and b) respectively. Silane conversion is logically low in the slug (about 50%) but high or even complete in the dense zones. As explained and illustrated in [17], a high flux of gas with low silane concentration penetrates through the bottom of the slug and the richer gas is evacuated towards its periphery. The convective and diffusive fluxes existing in these zones of high concentration gradients tend to impoverish the gas present in the slug progressively. Although Fig. 4(a) shows almost complete conversion of silane at the top of the bed at this run time, this is no longer the case after the slug erupts at the top, gas still relatively rich in silane will exit the reactor: the average conversion is therefore less than 100%. Fig. 4(b) shows that silylene is mainly produced in bubbles and slugs, in which the homogeneous chemistry is favoured, and it reaches a maximum mass fraction of only 3.6×10^{-7}. It is then about 10^5 times less concentrated in average than silane.

Fig. 5(a and b) presents the corresponding fields of Si deposition rates from silane and silylene respectively. Fig. 5(a) reveals that Si deposition from silane mainly occurs in the dense zones, at the bottom of the bed and between the slug and the group of bubbles. A significant part of this deposition process also occurs at the periphery of the slug due to the fluxes of "fresh gas" passing here as previously described. Silylene, which is mainly produced inside bubbles and slugs, mainly leads to Si deposition at their peripheries as shown by Fig. 5(b). However, a part of the deposition of Si from silylene can also occur in dense zones as revealed by the fixed bed simulation of the next section. The contribution of silylene to Si deposition can be as high as the contribution of silane locally,

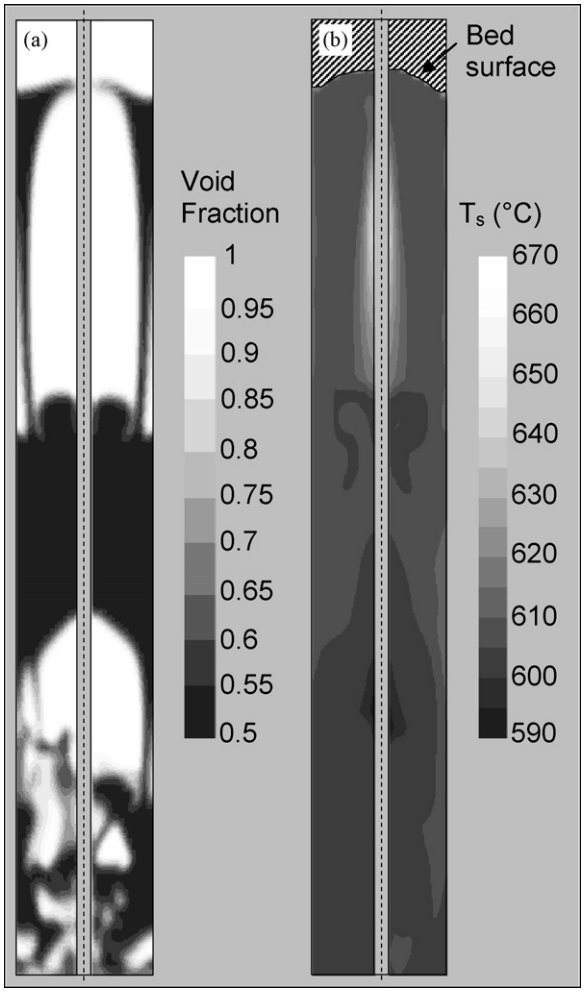

Fig. 3. Instantaneous fields (a) of void fraction and (b) of solid temperature for run A5 after 5 s of deposition.

as illustrated by Fig. 5(b). Therefore, the very low values of silylene concentrations are due to the very high heterogeneous kinetics of this species.

These simulations have shown that for highly reactive species such as SiH_2, concentration gradients appear at bubbles and slugs peripheries, where the deposition rate is high. So, one can think that species diffusion plays a significant role in these zones. Indeed, as shown by Fig. 6, values of the ratio between diffusive and convective fluxes in these zones are around 1. Therefore, the diffusion mass transfer can locally be as important as the convective one and then an accurate description of species diffusion is fully justified. However, on a global scale, calculations showed that the kind of model of diffusion used (constant dilute approximation or Wilke approximation, see Section 3.1) has no significant influence on the silane conversion. This is probably due to the fact that the residence time of the gas in the bed is too short to allow the diffusion process to play a very significant role.

5.2. Global results

The first two seconds of simulation were not considered, this was sufficient to prevent any transient phenomena to influence the data analysis. The six last seconds were more than required to get reliable and constant results averaged in time.

With the hydrodynamic model HM2, mean bed heights and mean heights of fluctuation calculated are around 31 and 9 cm

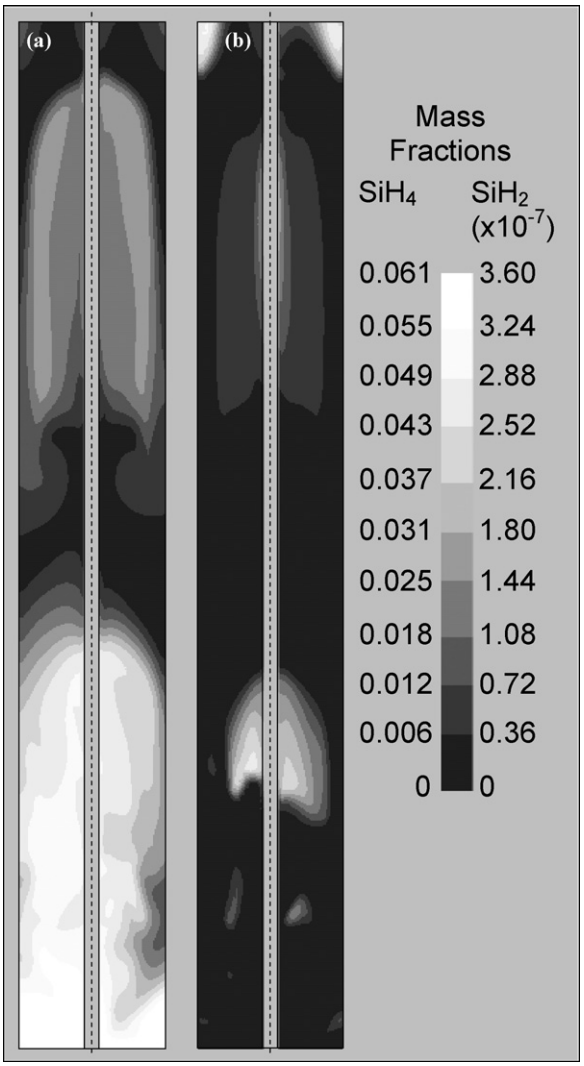

Fig. 4. Instantaneous fields (a) of silane and (b) of silylene mass fractions for run A5 after 5 s of deposition.

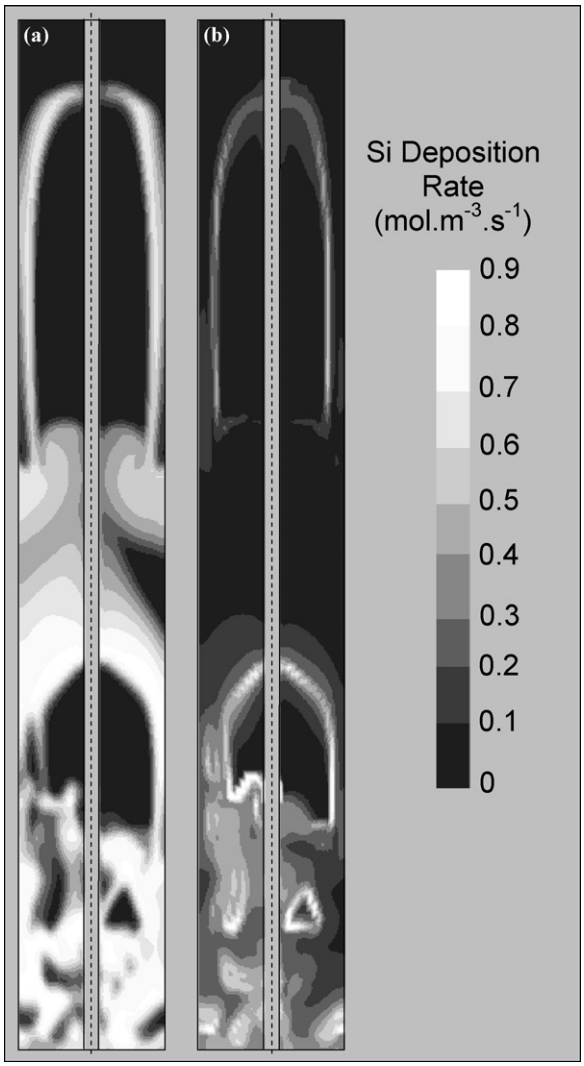

Fig. 5. Instantaneous fields of silicon deposition rate from (a) silane and (b) silylene for run A5 after 5 s of deposition.

respectively (except for run A12: 50 and 12.5 cm respectively), which gives bed expansions H/H_0 of about 1.45 and H/D ratios of about 6 (9.5 for run A12). These results are very close to those obtained with the same gas velocity and the same hydrodynamic model, but at ambient temperature (see [18]).

With the hydrodynamic model HM1, bed expansions are increased by 26% and heights of fluctuation by 44%. We did not find large discrepancies between results obtained with the Schaeffer/Princeton models in [18], where the true expression of the granular energy equation was always used; actually we have verified they are due here to the use of the approximated form of the granular energy equation in the model HM1. Model HM2 is obviously more reliable. This is the reason why it has been used for all the simulations performed using the three detailed models of chemistry, as indicated in Table 2.

Then, it is interesting to consider a spatially averaged instantaneous bed temperature defined as follows:

$$T_{bed} = \frac{1}{V_s} \int T_s \varepsilon_s \, dV \tag{15}$$

where V_s is the total volume of the solid phase, T_s its local temperature and ε_s the local solid void fraction. From the calculations, the mean bed temperatures vary regularly as a function of time and bed fluctuations, by 3–10 °C, with minima at maximum bed expansions and maxima at minimum bed expansions. The interaction between bed hydrodynamics and heat transfer in the bed are thus demonstrated. Time averages $\bar{T}_{bed}$ of these bed temperatures are reported in Table 2 for the five runs (it appeared that they were independent of the chemistry model and of the hydrodynamic model used). Except for run A12, they are lower than the mean temperatures measured in the inner tube and at the column walls (from 0 to 40 cm) by 5–11 and 24–28 °C respectively. This can be simply explained by the fact that the gas flow prevents the bed to become as hot as the walls. For run A12, the mean bed temperature calculated equals the mean temperature measured in the inner tube and is lower than the mean temperatures measured at the column walls by only 19 °C: as already explained in Section 2, the heat transfer is enhanced by the larger total surface of contact between the walls and the powders in this case.

In Table 2, the models GC-HM1 and GC-HM2 can be compared in terms of silane conversions. Since the HM1 hydrodynamic model overestimates bed fluctuations and then sizes of slugs, it logically underestimates the silane conversions compared to HM2, but by no more than 4.1% (run A12) and by 2.3% in average. Comparing the models FUR-HM1 and FUR-HM2, an opposite trend in found: FUR-HM1 tends to overestimate silane conversions. The reason is that the bigger slugs predicted by HM1 promote the silylene production and also the contribution of this species to deposition. Indeed, as

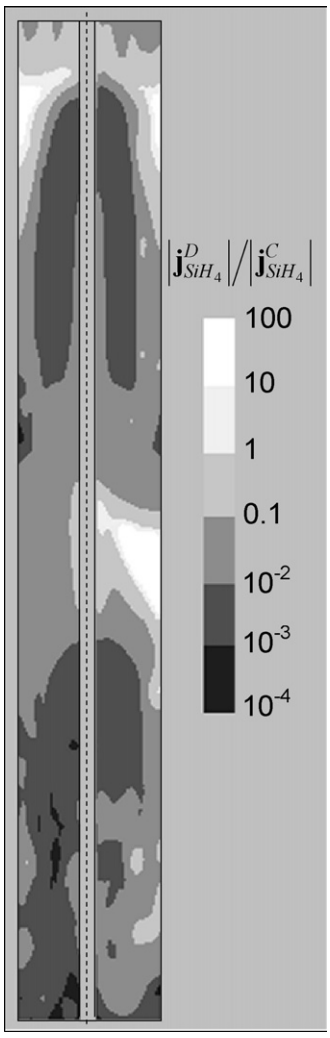

Fig. 6. Ratio of silane diffusive flux on silane convective flux for run A5 after 5 s of deposition.

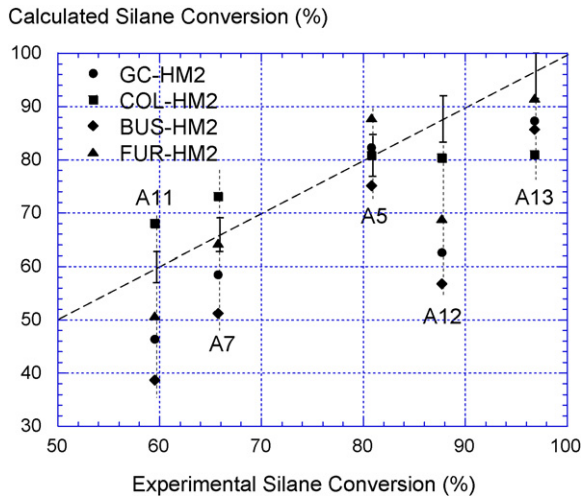

Fig. 7. Calculated silane conversions *vs.* experimental silane conversions.

can be seen in Table 2, with FUR-HM1, the contribution of silane to deposition is significantly lower than with FUR-HM2, by 6.4% in average. Therefore, the interactions between the bed hydrodynamics and the chemistry are significant and the former must be modelled as precisely as possible to obtain good predictions about chemistry and deposition phenomena.

In Fig. 7, the silane conversions calculated by the models GC-HM2, COL-HM2, BUS-HM2 and FUR-HM2 are compared to the experimental silane conversions. Excepted for run A5, GC-HM2 and FUR-HM2 underestimate silane conversions. The average discrepancy of silane conversion is of 11.3% with GC-HM2 and it decreases to 8.2% with FUR-HM2. BUS-HM2 underestimates silane conversions for all runs and the average discrepancy is of 16.6%. With COL-HM2, the average discrepancy is only of 7.8%. However, it cannot be concluded that COL-HM2 is the best model. Indeed, regarding the differences between minimum and maximum silane conversions, an experimental value of 37% is found, GC-HM2 and FUR-HM2 gives a value of 41%, BUS-HM2 a value of 47% and COL-HM2 a value of only 13%. Thus, COL-HM2 leads to nearly constant silane conversions that do not follow the experimental trend; the activation energy of kinetics (5) is probably too low.

Because kinetics (8) is lower than kinetics (1), BUS-HM2 predicts higher contributions of silylene to deposition than FUR-HM2, the former with values around 30% and the latter with values around 25%, but the trends are similar with a maximum silylene contribution for run A7 (the run with the maximum SiH_4 inlet mass fraction) and a minimum one for run A13 (the run with the minimum SiH_4 inlet mass fraction). These evolutions are analysed in the next section.

Note that if the chemical model FUR is run in a fixed bed, i.e. in the same operating conditions as those used by Furusawa et al. [9] to determine the kinetics (1), some silylene is produced by the reaction (R_1) and its contribution to the deposition is of about 30%. This means that the kinetics (1) includes intrinsically a contribution of silylene to deposition and that the model FUR would tend to intrinsically overestimate the total deposition rate.

5.3. *Effects of temperature and inlet silane concentration on silylene contribution to the deposition*

Whatever the chemical model used, FUR-HM2 or BUS-HM2, by comparing the different runs (in particular run A7 and run A13),

Table 2
Inlet mass fractions and simulation results.

Run	Calculated $\bar{T}_{bed}$ (°C)	$X^0_{SiH_4}$	Measured silane conversion (%)	Calculated silane conversion (%) – contribution of silane to deposition (%)					
				GC-HM1	FUR-HM1	GC-HM2	COL-HM2	BUS-HM2	FUR-HM2
A5	610	0.0615	80.8	83–100	87.4–80.9	82.3–100	80.8–79.8	75.1–71.4	87.9–84.5
A7	598	0.1185	65.7	55.5–100	68.9–68.8	58.5–100	73.2–85	51.2–62.1	64.3–78.3
A11	574	0.077	59.5	44.1–100	55.5–74.2	46.4–100	68.1–90.7	38.7–70.8	50.8–82.8
A12[a]	573	0.078	87.7	58.5–100	68–76.3	62.6–100	80.4–90.6	56.8–73.7	68.9–83.9
A13	605	0.0275	96.8	84.5–100	89–86.1	87.3–100	81–80.3	85.7–81.9	91.6–88.6
S1	605	0.077	–	–	–	–	–	63.6–70.6	81.9–82.8
S2	675	0.077	–	–	–	–	–	99.8–60.6	99.9–79.3

[a] 1300 g of powder, 800 g for the other runs.

it appears clearly that the lower the inlet mass fraction of silane, the higher the contribution of this species to deposition and the lower the contribution from SiH_2. This can be easily explained by the fact that the apparent order of the heterogeneous reaction of Si deposition from silane (whatever its kinetics (1) or (8)) is lower than the order 1 of reaction (R_1).

Regarding the temperature, the situation is uncertain, the present runs do not allow to clearly determine its effect on the silane contribution to deposition. This is why two additional runs were simulated, S1 and S2, with the same inlet mass fraction of silane as run A11, but applying the temperature boundary conditions of A13 for S1 and those of A5 plus 65 °C for S2, which led to mean bed temperatures $\bar{T}_{bed}$ of 605 and 675 °C for S1 and S2 respectively whereas $\bar{T}_{bed}$ calculated for run A11 was of 574 °C (see Table 2). As a result, with the model FUR-HM2, no significant variation of silane contribution to deposition is found. With the model BUS-HM2, a significant decrease of the silane contribution to deposition is observed for the high temperature of run S2, which can be logically explained by the fact that the activation energy of reaction (R_1) is higher than that of kinetics (8).

6. Conclusion

The silicon fluidized bed CVD process from SiH_4 in transient conditions has been modelled using the multifluid Eulerian code MFIX.

A preliminary experimental study has been performed using an alumina powder of 329 μm in Sauter diameter. The results obtained have been used as a database for the model validation.

In the operating range considered, homogeneous and heterogeneous kinetic models available in the literature for silicon deposition from silane have been analysed and compared. Four of them have been retained and implemented in the MFIX code: the purely heterogeneous Furusawa model (GC), and three models considering both homogeneous and heterogeneous chemistries (COL, BUS and FUR), respectively derived from the works of Coltrin, Buss and Furusawa.

3-D modelling of the fluidized bed has been performed by applying the experimentally measured thermal profiles and by testing two hydrodynamic models.

A limitation of the Eulerian approach has been emphasized: at the particle scale, transport (diffusional or convective) limitations exist for highly reactive species like silylene (SiH_2). These transport limitations cannot be considered in Eulerian models, resulting in an overestimated heterogeneous consumption of silylene and thus reducing drastically the role of polysilanes for the conditions tested. As a consequence, we assumed that silylene represents all the homogeneous species formed during silane pyrolysis.

Instantaneous fields of void fraction, temperature of solids, SiH_4 and SiH_2 mass fractions and deposition rates have been analysed for given operating conditions. Results showed a strong interaction between the bed hydrodynamics, thermal and reactive mass transfers. Si deposition from SiH_4 mainly occurs in dense zones of the bed. SiH_2 forms in bubbles and slugs and leads to Si deposition at their periphery. The contribution of SiH_2 to the deposition can locally be as high as the contribution of SiH_4. Sharp concentration gradients exist at slug peripheries which promotes diffusive transfer of species in these zones.

Finally, by comparing the simulated silane conversions with experimental ones, the activation energy of the heterogeneous kinetics of the model COL revealed to be too low for the conditions tested. Better agreements have been obtained using the models GC, BUS and FUR. The average contribution of SiH_2 to Si deposition clearly increases with the inlet concentration of SiH_4 and can reach values as high as 30%.

The whole results obtained demonstrate the necessity to accurately represent not only the chemical reactions but also the hydrodynamics and heat transfer to perform convenient simulations of a FBCVD process.

Acknowledgements

We acknowledge Sreekanth Pannala and Madhava Syamlal for MFIX support and helpful discussions. Simulations presented in this paper were carried out with the help of I. Touche from LGC, using (i) the Grid'5000 experimental test, an initiative from the French Ministry of Research through the ACI GRID incentive action, INRIA, CNRS and RENATER and other contributing partners (see https://www.grid5000.fr), and (ii) the French supercomputing centers CalMip and CINES. This project has been supported by the French ANR-Réseau National Matériaux et Procédés.

References

[1] J. Pina, V. Bucala, P. Ege, H. de Lasa, Int. J. Chem. Reactor Eng. 4 (2006) 1–21.
[2] M.P. Tejero-Ezpeleta, S. Buchholz, L. Mleczko, CJChE 82 (2004) 520–529.
[3] C.M. White, P. Ege, B.E. Ydstie, Powder Technol. 163 (2006) 51–58.
[4] S. Lai, P. Dudukovic, P.A. Ramachandran, Chem. Eng. Sci. 41 (1986) 633–641.
[5] K. Kato, C.H. Wen, Chem. Eng. Sci. 24 (1969) 1351–1368.
[6] T.R. Hogness, T.L. Wilson, W.C. Johnson, J. Am. Chem. Soc. 58 (1936) 108–112.
[7] S.K. Iya, R.N. Flagella, F.S. DiPaolo, J. Electrochem. Soc. 129 (1982) 1531–1535.
[8] G. Hsu, R. Hogle, N. Rohatgi, A. Morrison, J. Electrochem. Soc. 131 (1984) 660–663.
[9] T. Furusawa, T. Kojima, H. Hiroha, Chem. Eng. Sci. 43 (1988) 2037–2042.
[10] D. Kunii, O. Levenspiel, Ind. Eng. Chem. Res. 29 (1990) 1226–1234.
[11] B. Caussat, M. Hemati, J.P. Couderc, Chem. Eng. Sci. 50 (1995) 3615–3624.
[12] F. Fayolle, Analyse et modélisation des dépôts d'oxyde de silicium par procédé LPCVD, Ph.D. Thesis, I.N.P. Toulouse, Toulouse, France, 1993.
[13] J. Pina, V. Bucala, S.N. Schbib, P. Ege, H.I. de Lasa, Fluidization XII, Vancouver, Canada, 2007.
[14] B. Van Wachem, J.C. Schouten, C.M. Van den Bleek, R. Krishna, J.L. Sinclair, AIChE J. 47 (2001) 1035–1051.
[15] C. Guenther, T. O'Brien, M. Syamlal, Fourth International Conference on Multiphase Flow, New Orleans, LA, USA, 2001.
[16] www.mfix.org.
[17] L. Cadoret, N. Reuge, S. Pannala, M. Syamlal, C. Coufort, B. Caussat, Surf. Coat. Technol. 201 (2007) 8919–8923.
[18] N. Reuge, L. Cadoret, C. Coufort, S. Pannala, M. Syamlal, B. Caussat, Chem. Eng. Sci. 63 (2008) 5540–5551.
[19] S. Benyahia, M. Syamlal, T.J. O'Brien, Summary of MFIX Equations 2005-4, From URL http://www.mfix.org/documentation/MfixEquations2005-4-1.pdf, 2006.
[20] M. Syamlal, T.J. O'Brien, AIChE J. 49 (2003) 2793–2801.
[21] M. Syamlal, W. Rogers, T.J. O'Brien, MFIX documentation: Theory guide, Technical Report DOE/METC-94/1004 (DE9400087), (can be downloaded from: http://www.mfix.org) Morgantown Energy Technology Centre, Morgantown, West Virginia, 1993.
[22] D.G. Schaeffer, J. Differential Equations 66 (1987) 61–74.
[23] A. Srivastava, S. Sundaresan, Powder Technol. 129 (2003) 72–85.
[24] S.V. Patankar, Numerical Heat Transfer and Fluid Flow, Hemisphere Series on Computational Methods in Mechanics and Thermal Science, Hemisphere Publishing Corporation, Washington, DC, USA, 1980.
[25] R. Barrett, M. Berry, T. Chan, J. Demmel, J. Donato, J. Dongarra, V. Eijkhout, R. Pozo, C. Romine, H. van der Vorst, Templates for the Solution of Linear Systems: Building Blocks for Iterative Methods (this book is available at http://www.netlib.org/templates/templates.pdf), 2nd edition, SIAM Publishing, Philadelphia, PA, USA, 2006.
[26] M. Syamlal, MFIX Documentation: Numerical technique, Technical Report DOE/MC31346-5824 (DE98002029) (can be downloaded from http://www.mfix.org), Morgantown Energy Technology Centre, Morgantown, West Virginia, 1998.
[27] L. Cadoret, N. Reuge, S. Pannala, M. Syamlal, C. Rossignol, J. Dexpert-Ghys, C. Coufort, B. Caussat, Powder Technol., in press.
[28] R. Siegel, J.R. Howell, Thermal Radiation Heat Transfer, Hemisphere Publishing Corporation, Washington, DC, USA, 1992.
[29] C.R. Wilke, Chem. Eng. Prog. 46 (1950) 95–104.
[30] R. Taylor, R. Krishna, Multicomponent Mass Transfer, John Wiley and Sons, New York, USA, 1993.
[31] K. Terzaghi, Theoretical Soil Mechanics, Wiley, New York, NY, USA, 1942.
[32] P.C. Johnson, R. Jackson, J. Fluid Mech. 176 (1987) 67–93.
[33] T. Kojima, T. Kimura, M. Matsukata, Chem. Eng. Sci. 45 (1990) 2527–2534.
[34] N.K. Rohatgi, G.C. Hsu, R. Lutwack, Proc. Symp. Electrochem. Soc. Montreal (1982) 477–487.
[35] G. Hsu, N. Rohatgi, J. Houseman, AIChE J. 33 (1987) 784–791.
[36] M.E. Coltrin, R.J. Kee, G.H. Evans, J. Electrochem. Soc. 136 (1989) 819–829.

[37] A. Dollet, S. de Persis, F. Teyssandier, Phys. Chem. Chem. Phys. 6 (2004) 1203–1212.
[38] P. Ho, M.E. Coltrin, W.G. Breiland, J. Phys. Chem. 98 (1994) 10138–10147.
[39] D.M. Kremer, R.W. Davis, E.F. Moore, S.H. Ehrman, J. Cryst. Growth 247 (2003) 333–356.
[40] D.M. Kremer, R.W. Davis, E.F. Moore, S.H. Ehrman, Chem. Eng. Sci. 59 (2004) 1115–1130.
[41] S. Nijhawan, P.H. McMurry, M.T. Swihart, S.-M. Suh, S.L. Girshick, S.A. Campbell, J.E. Brockmann, Aerosol Sci. 34 (2003) 691–711.
[42] C.R. Kleijn, Thin Solid Films 365 (2000) 294–306.
[43] R.F.C. Farrow, J. Electrochem. Soc. 121 (1974) 899–907.
[44] C.H.J. Van den Brekel, Ph.D. Thesis, University of Nijmegen, Nijmegen, The Netherlands, 1978.
[45] M.E. Coltrin, R.J. Kee, J.A. Miller, J. Electrochem. Soc. 133 (1986) 1206–1213.
[46] M.E. Coltrin, R.J. Kee, F.M. Rupley, E. Meeks, Surface Chemkin III, (to be obtained from: Reaction Design, Inc., 11436 Sorrento Valley Road, San Diego, CA 921121, USA), Technical Report SAND96-8217, Sandia National Laboratories, Albuquerque, NM/Livermore, CA, USA, 1996.
[47] R.J. Buss, P. Ho, W.G. Breiland, M.E. Coltrin, J. Appl. Phys. 63 (1988) 2808–2819.
[48] Y.B. Wang, F. Teyssandier, J. Simon, R. Feurer, J. Electrochem. Soc. 141 (1994) 824–842.
[49] W.G. Breiland, M.E. Coltrin, J. Electrochem. Soc. 137 (1990) 2313–2319.
[50] W.A.P. Claassen, J. Bloem, W.G.J.N. Valkenburg, C.H.J. van den Brekel, J. Cryst. Growth 57 (1982) 259–266.
[51] D.W. Foster, A.J. Learn, T.I. Kamins, J. Vac. Sci. Technol. 4 (1986) 1182–1186.
[52] R.S. Rosler, Solid State Technol. (1977) 63.
[53] H.K. Moffat, K.F. Jensen, J. Electrochem. Soc. 135 (1988) 459–471.
[54] S.M. Gates, B.A. Scott, D.B. Beach, R. Imbihl, J.E. Demuth, J. Vac. Sci. Technol. 5 (1987) 628–630.
[55] W.L.M. Weerts, M.H.J.M. de Croon, G.B.M.M. Marin, J. Electrochem. Soc. 145 (1998) 1318–1330.